Response of Intensity and Structure of Typhoon Jebi (2018) before Landfall to 2-K and 4-K Warmed Future Climates in Dynamical Downscaling Experiments

Keita Fujiwara, Tetsuya Takemi, and Nobuhito Mori

Disaster Prevention Research Institute, Kyoto University, Kyoto, Japan

(Manuscript received 12 February 2023, accepted 21 May 2023)

Abstract To investigate the effects of global warming on Typhoon Jebi (2018), we performed high-resolution pseudo-global 2-K and 4-K warming simulations with initial time ensembles using a regional atmospheric model. The pseudo-global warming experiments demonstrated the further facilitation of Jebi's development with a higher rise in the temperature. The intensity over the ocean to the south of Japan increased by 8% (20%) in the climate warmed 2-K (4-K) to the current climate. Typhoon Jebi, in the 4-K warming simulations, maintained a robust inner-core characterized by a compact and deep eyewall and well-developed primary and secondary circulations even immediately before landfall, in contrast to the result in the 2-K warming simulations. The sustained robust axisymmetric structure immediately before landfall in the 4-K warming runs was strongly associated with the enhanced ocean warming around Japan, notable moistening of the lower-to-middle troposphere in the vicinity of Typhoon Jebi, and a significant decrease in vertical wind shear under the extremely warmed future climate. The nonlinear responses of Typhoon Jebi to the tropospheric temperature rise are attributable to the drastic changes in the midlatitude's thermodynamic and dynamic environments under climate changes resulting from 2-K to 4-K global warming.

Citation: Fujiwara, K., T. Takemi, and N. Mori, 2023: Response of intensity and structure of Typhoon Jebi (2018) before landfall to 2-K and 4-K warmed future climates in dynamical downscaling experiments. *SOLA*, **19**, 142−149, doi:10.2151/sola.2023-019.

1. Introduction

The effects of climate change on devastating tropical cyclones (TCs) are one of today's greatest concerns both in the scientific community and in the field of societal risk assessment. The intensity of TCs is critically affected by the sea surface temperature (SST) conditions (Demaria and Kaplan 1994; Emanuel 1988). The Fifth Assessment Report of the Intergovernmental Panel on Climate Change (IPCC) reported that global warming has caused a worldwide increase in SSTs (IPCC 2013, 2014). Modeling studies have indicated an increase in the number of intense TCs due to the SST increase under the global-warming climate (e.g., Oouchi et al. 2006; Murakami et al. 2012; Murakami and Sugi 2010).

The SST increase in the future climate is expected to be greater at higher latitudes (Mizuta et al. 2017), leading to a northward shift of the location of TC maximum intensity (Kossin et al. 2014, 2016; Yoshida et al. 2017). High-resolution future simulations have projected greater occurrences of category 4 and 5 TCs on the Saffir–Simpson scale around Japan (Kanada et al. 2013; Tsuboki et al. 2015). Kanada et al. (2020) indicated that the warming climate will facilitate the development of TCs at higher latitudes as a result of changes in thermodynamic and dynamic environments in response to future climate changes. Thus, mid-to-high-latitude countries, such as Japan, will face an increasing threat of TCs in the future.

Recently, an extreme TC, Typhoon Jebi (2018), induced serious damage to western Japan comparable to that induced by the most threatening previous TCs, such as Typhoon Nancy in 1961 and the Muroto Typhoon in 1934, because of catastrophic wind gusts and storm surge (Mori et al. 2019; Takemi et al. 2019). Jebi reached its maximum intensity over the midlatitude ocean south of Japan (915 hPa and 105 knots according to the Regional Specialized Meteorological Center Tokyo) and made landfall on the Pacific coast of western Japan while retaining the greatest power for a TC in the previous 25 years (1994–2018). Given the effects of global warming on TC intensity, examining how the future warming climate would affect Jebi is important for preparing for an anticipated worst-class natural disaster. Therefore, Jebi should be a useful case study for investigating the effects of global warming on a worst-class typhoon. In addition, recent modeling studies of TCs approaching Japan under a future climate have focused mainly on TC behaviors under extreme warming environments based on the Representative Concentration Pathway 8.5 scenario (e.g., Kanada et al. 2020; Nayak and Takemi 2019; Takemi 2019). The impact of climate change on TCs will be better understood if we consider various warming scenario such as moderate global warming.

Here, we investigate the response of Jebi (2018) to future climates with moderate and extreme warming. To achieve

Corresponding author: Keita Fujiwara, Disaster Prevention Research Institute, Kyoto University, Gokasho, Uji, Kyoto 611-0011, Japan. E-mail: fujiwara.keita.7p@kyoto-u.ac.jp.

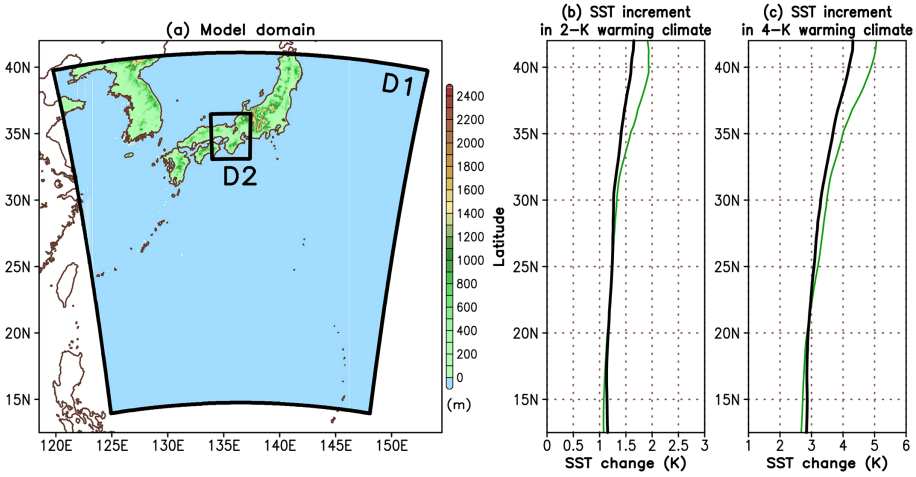

Fig. 1. (a) Domain for the WRF simulations with the terrain height above sea level (shading). (b and c) Zonal-mean SST increment in September, as derived from the (a) 2-K and (b) 4-K warming future climate. The green and black lines denote the WNP-mean and global-mean values, respectively.

this purpose, we conducted downscaling pseudo-global warming (PGW) simulations using a high-resolution atmospheric model. In the PGW method, the climate changes derived from a global climate model (Mizuta et al. 2012, 2017) were added to the initial and boundary conditions in the current climate state to quantify the effects of a future climate warming on Jebi.

2. Numerical model and design of the control and PGW runs

Both the control (CTL) and PGW runs of Jebi were conducted using the Weather Research and Forecasting (WRF) model (Skamarock et al. 2008) version 3.9.1. The WRF model used two-way nested domains giving a 5-km horizontal mesh (D1) and a 1-km horizontal mesh (D2) (Fig. 1a). The cloud microphysics scheme, planetary boundary layer (PBL) and surface schemes, and short and long wave radiation scheme were applied by the WRF Single-Moment 6-Class Scheme (Hong and Lim 2006), Yonsei University Scheme (Hong 2010; Hong et al. 2006), and Rapid Radiative Transfer Model Scheme (Dudhia 1989; Mlawer et al. 1997), respectively. Cumulus parameterization was not used for D1 and D2. These settings were the same as the previous study (Takemi et al. 2019).

The initial and boundary conditions of the atmosphere and SST were derived from the 1-degree-horizontal-mesh and 6-hourly National Center for Environmental Prediction (NCEP) Final Operational Global Analysis (FNL). SST condition was updated daily by the NCEP FNL. Given the uncertainties of numerical simulations, we conducted initial time ensemble experiments for D1 and D2. The 16 different initial times for D1 were 0000, 0600, 1200, and 1800 UTC on each day from 30 August to 2 September 2018, and the end time of all the simulations was 1200 UTC on 4 September 2018. A spectral nudging for wave-number components of 2 was applied only for zonal and meridional winds above a height of approximately 750 hPa in D1. The 16 ensemble simulations also were performed for D2 during the period from 0000 to 1200 UTC on 4 September 2018 to assess the local hazards by Typhoon Jebi under the warming scenario, which will be addressed in a separate paper. In this study, we analyzed only D1 results.

In the PGW simulations, we used the database for Policy Decision making for Future climate change (d4PDF), having a large ensemble of 60-km-resolution global climate simulations for the current climate and for future climates with 2-K and 4-K warming (Fujita et al. 2018; Mizuta et al. 2017). The PGW increments were defined as the differences in monthly mean values of August or September between the present (1981–2010) and future (2051–2080) climate and were zonally uniform values on the p-levels and surface. The zonal-mean increments of SST, pressure-level temperature, and surface temperature, which have been predicted to change significantly in the future climate (Takemi 2012), were added to the initial and boundary conditions of the CTL run. Wind increments were not added to reduce undesirable changes in the track of Jebi in the PGW runs (Takemi et al. 2016). The SST warming over the western North Pacific (WNP) in the midlatitudes was more pronounced than the global-mean value (Japan Meteorological Agency 2018). Therefore, the aforementioned zonal-mean increments were estimated within the WNP sector (110°E–180°E). The difference in the zonal-mean SST increment between the WNP-mean and global-mean was evident north of 30°N (Fig. 1b). In the PGW runs, the tropospheric temperature increment over the WNP indicates a more stabilized condition (Fig. S1). For convenience, the 2-K (4-K) warming future climate simulation is hereafter referred to as the PGW2 (PGW4) run.

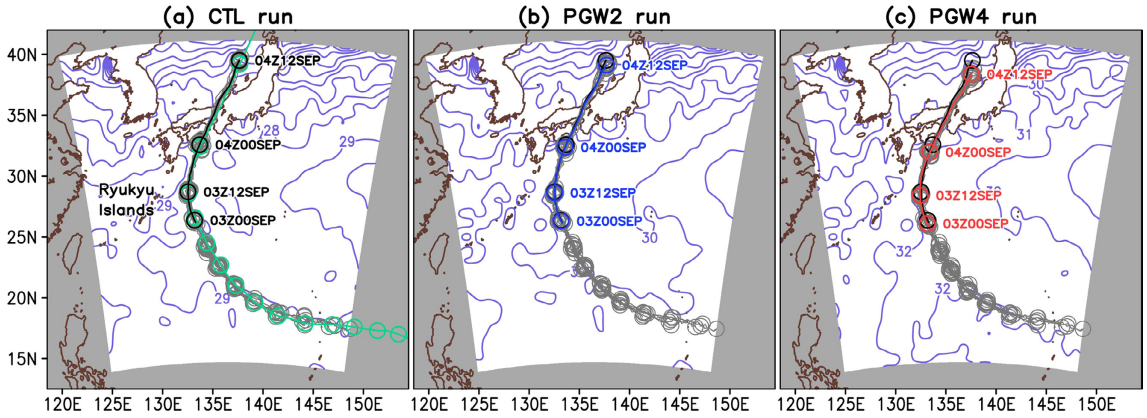

Fig. 2. (a) Track of Jebi derived from the best track data (green line) and each ensemble simulation (gray lines) in the CTL run. The ensemble-mean track from 0000 UTC 3 September to 1200 UTC 4 September is drawn by a black line. The opened circles show the TC positions at 0000 and 1200 UTC on each day. Purple contours with 1°C intervals denote the SST condition on 3 September. (b) Same as in Fig. 2a but for the PGW2 run. The ensemble-mean track in the CTL and PGW2 runs is also illustrated by black and blue lines, respectively. (c) Same as in Fig. 2b but for the PGW4 run. The ensemble-mean track in the CTL and PGW4 runs is also illustrated by black and red lines, respectively.

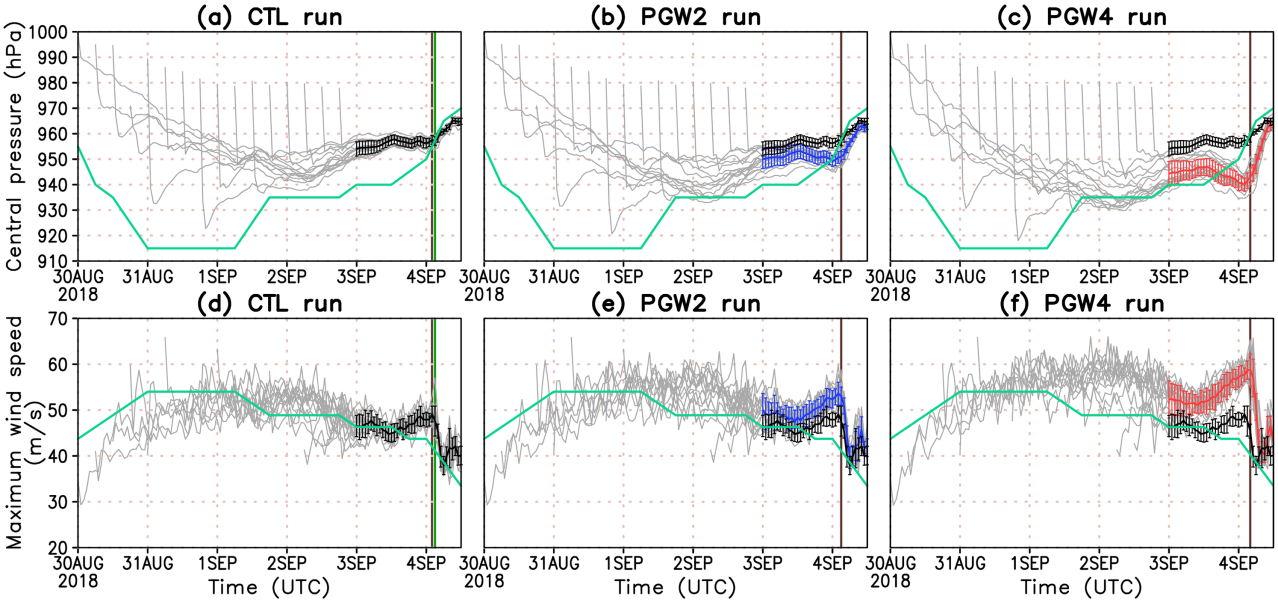

Fig. 3. (a) Time series of the central pressure of Jebi, as derived from the best track data (green line), and ensemble simulations in the CTL run (gray lines). The ensemble-mean intensity from 0000 UTC 3 September to 1200 UTC 4 September is drawn by a black line. Error bars denote the one standard deviation. Vertical bars denote the time of landfall based on the best track data (green line) and ensemble-mean track in the CTL run (brown line). (b) Same as in Fig. 3a but for the PGW2 run. The blue line denotes the ensemble-mean intensity in the PGW2 run. (c) Same as in Fig. 3a but for the PGW4 run. The red line denotes the ensemble-mean intensity in the PGW4 run. (d–f) Same as in Figs. 3a–3c but for the wind speed of Jebi.

3. Results

Figure 2 shows the track of Jebi (2018) derived from the best track data and simulations, along with the SST conditions on 3 September. The simulated TC centers were detected as the grid where the sea level pressure (SLP) was minimum. The best track data recorded the northward migration of Jebi over the ocean east of the Ryukyu Islands, where the SST was approximately 29°C, and the landfall in western Japan on 4 September (Fig. 2a). The CTL run roughly followed the observed path because of the spectral nudging. The root mean square error of track is 0.17° (0.22°) in longitude (latitude) during the period from 0000 UTC on 3 to 0000 UTC on 4 September. The PGW-simulated track resembled that in the CTL run although the PGW4 run decreased the translation speeds around Japan compared with those in the CTL run (Fig. S2). In the PGW2 and PGW4 runs, TCs passed the warm SST regions at ~30°C and ~32°C, respectively.

Figure 3 shows the time series of central pressure and wind speed of Jebi derived from the best track data and sim-

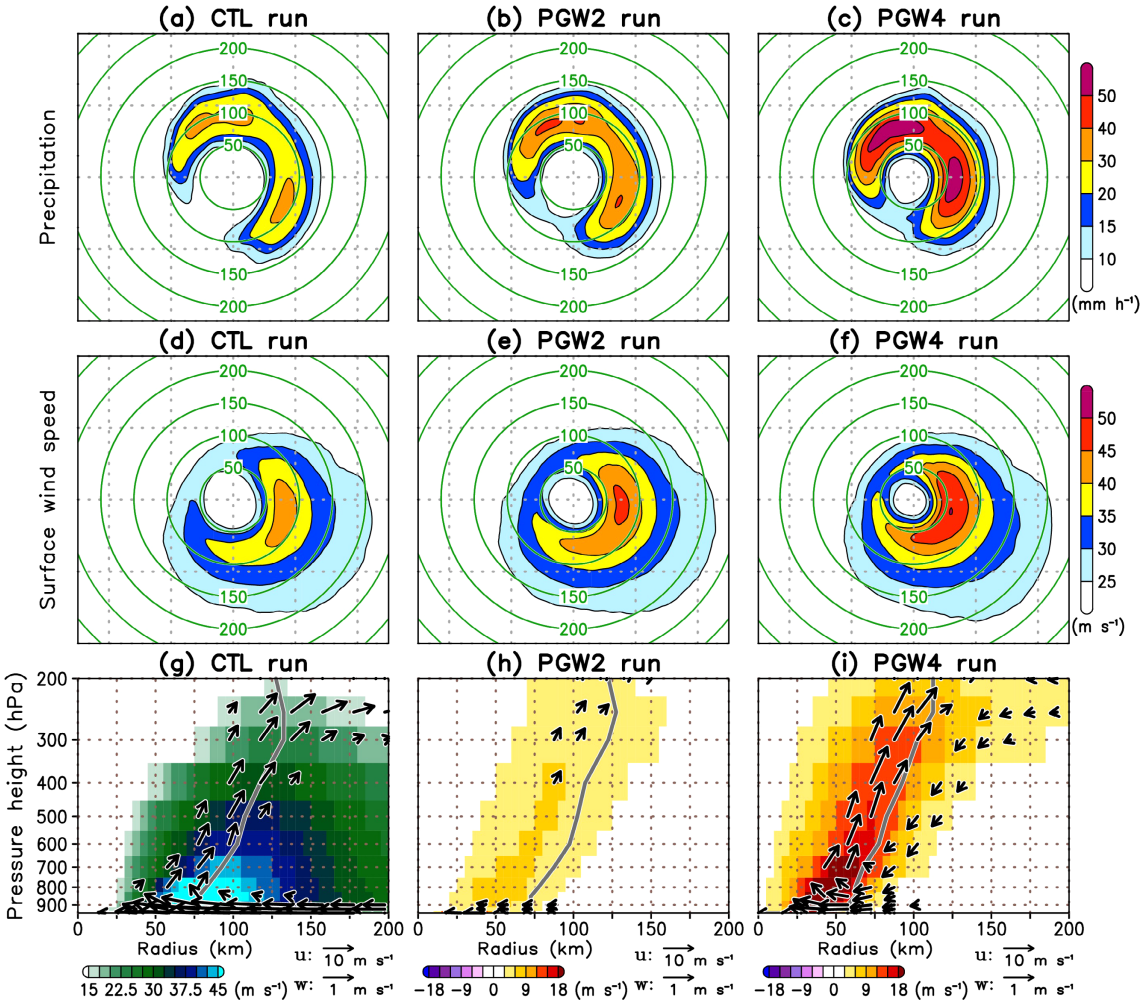

Fig. 4. (a–c) Ensemble-mean horizontal maps of center-composite mean precipitation in the (a) CTL, (b) PGW2, and (c) PGW4 runs during the re-intensification phase. Contours with intervals of 50 km denote the radius from the TC center. (d–f) Same as in Figs. 4a–4c, but for the surface wind speed. (g–i) Ensemble-mean radial-height cross sections of the azimuthal-mean tangential wind speed (shading) and secondary circulation (vectors) in the (g) CTL, (h) PGW2, and (i) PGW4 runs. Each variable is averaged during the re-intensification phase. The gray line denotes the simulated RMW. Vectors of secondary circulation less than 2 m s^{-1} are not drawn. Note that the shading and vectors in the PGW2 (PGW4) runs denote the differences between PGW2 (PGW4) and CTL runs (the former and the latter). Difference vectors less than 2 m s^{-1} are not drawn.

ulations. The CTL-simulated intensity was somewhat different from the best track data when TCs were located to the east of the Ryukyu Islands; however, the temporal evolutions of SLP and wind speed before Jebi's landfall in the CTL run were very similar to those at some observatories (see Fig. S3). The comparison between the CTL run and in-situ observation supported that the reproducibility of the CTL run was sufficient to examine the behaviors of Jebi at least at times around the landfall. The PGW runs indicated the re-intensification immediately before landfall (Figs. 3b, 3c, 3e, and 3f). Interestingly, the re-intensification was more evident with a higher rise in the tropospheric temperature. The minimum central pressure around Japan was 956.1 ± 1.7, 949.3 ± 2.1, and 940.0 ± 2.6 hPa in the CTL, PGW2, and PGW4 runs, respectively. The range means one standard deviation. The PGW2 (PGW4) run increased the ensemble-mean maximum wind speeds by ~8% (~20%) with respect to the CTL run when TCs were located over the ocean south of Japan: 49.1 ± 1.7, 53.2 ± 2.5, and 58.7 ± 3.5 m s^{-1} in the CTL, PGW2, and PGW4 runs, respectively.

To explore why a significant increase in the TC intensity occurred in the 4-K warming scenario but not in the 2-K warming scenario, we examined the inner-core structures of Jebi during the re-intensification phase. The re-intensification phase was simply defined as the 6-hourly periods prior to the time when the TC wind speed reached its maximum immediately before landfall (i.e., from 2000 UTC on 3 September to 0200 UTC on 4 September in the CTL and PGW2 runs and from 2200 UTC on 3 September to 0400 UTC on 4 September in the PGW4 run).

Figures 4a–4c and 4d–4f shows the center-composite mean horizontal maps of precipitation and surface wind speed during the re-intensification phase, respectively. The CTL run indicated asymmetric distributions of severe precipitation (e.g., ~30 mm h^{-1}) and strong wind (e.g., ~40 m s^{-1}) in a narrow area of inner-core region. The PGW2 and PGW4 runs

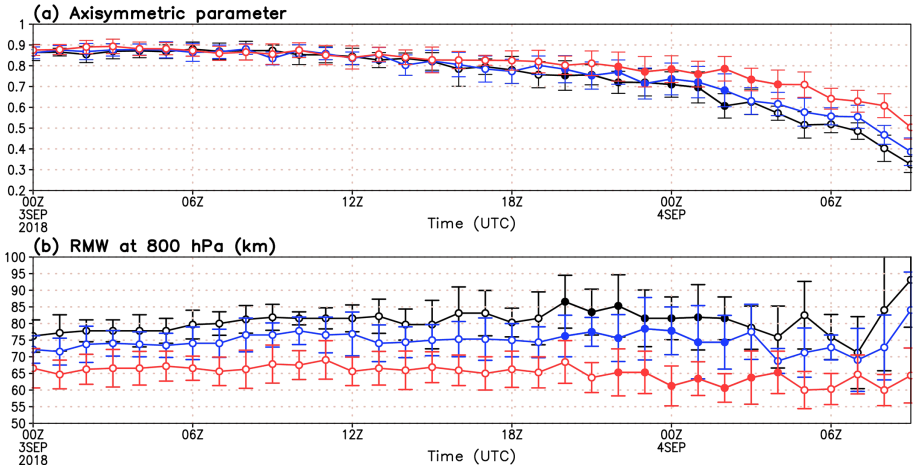

Fig. 5. Time series of the ensemble-mean (a) axisymmetric parameter and (b) RMW at 800 hPa derived from CTL (black line), PGW2 (blue line), and PGW4 (red line) runs. Error bars denote the one standard deviation. Closed marks denote the re-intensification phase.

clearly exhibited decrease in the size of TC eye and large increases in precipitation and surface wind around the eye. Such structure changes of TCs in the warming scenario agreed with the features reported in previous studies for TCs under global warming (Kanada et al. 2013, 2017; Wang et al. 2015).

Figures 4g–4i displays the radius-height cross sections of the azimuthal-mean tangential wind speed and the TC secondary circulation during the re-intensification phase. The CTL run simulated the outward-tilting eyewall (Fig. 4g). The PGW4 run showed more robust inner-core structures characterized by the smaller radius of maximum wind speed (RMW) and more compact and taller eyewall than those in the CTL run (Fig. 4i). The tangential flows were also remarkably enhanced by in the lower troposphere with respect to those in the CTL run. In the PGW2 run, the inner-core spin-up was unclear compared with the structure in the 4-K warming scenario (Fig. 4h). A large difference between the PGW2 and PGW4 runs was originated from the inward advection of the absolute angular momentum (AAM) in the PBL (Fig. S4). In the PGW4 run, the well-developed inflow largely enhanced the radial AAM advection around the RMW. The PGW2 run showed a little increase in the radial AAM advection because of the small inflow reinforcement. This result confirms that the incredibly robust inner-core structures in the PGW4 runs are responsible for the significant increase in the radial AAM advection due to enhanced secondary circulations around the eyewall.

To further investigate the differences in the robustness of the TC inner core between the CTL and PGW runs, we showed the time history of the RWM at 800 hPa and axisymmetric parameter in Fig. 5. The axisymmetric parameter, $\alpha(r,z,t)$, defined by Miyamoto and Takemi (2013) was computed as

$$\alpha(r,z,t) = \frac{\bar{\phi}(r,z,t)^2}{\bar{\phi}(r,z,t)^2 + \int \phi'(r,\theta,z,t)^2 d\theta/2\pi},$$

where $\bar{\phi}(r,z,t)$ and $\phi'(r,\theta,z,t)$ denote the axisymmetric and asymmetric components of a variable ϕ, respectively, and r, θ, and z represent the radial, tangential, and vertical directions, respectively. If $\alpha = 1$, the TC has a fully axisymmetric structure. In this study, α was obtained using tangential wind speeds and was averaged within a radius of 100 km from the TC center and at pressure levels between 200 and 925 hPa. In the CTL run, α (RMW) decreased (increased) gradually as Jebi migrated northward, indicating that the axisymmetric structures began to collapse in baroclinic zones with a lower SST around Japan. Similar trends of α and RMW to the CTL run were also seen in the PGW2 run. As expected on the basis of Fig. 4i, the PGW4 run showed a slower α decrease. Furthermore, the RMW reached its minimum value in the re-intensification phase immediately before landfall. These results indicate that Jebi makes landfall in western Japan while maintaining its robust and axisymmetric inner-core structure under the extremely warming climate.

To reveal why the PGW4 run maintained the robust axisymmetric structures around Japan (Figs. 4i and 5), we investigated the environmental parameters in the vicinity of Jebi. The environmental parameters were the SST, surface turbulent latent heat flux (LHF), 925-hPa water–vapor mixing ratio (Qv925), maximum convective available potential energy for an air parcel with max theta-e within low levels released from a height of 500 m (mCAPE), 500-hPa water–vapor mixing ratio (Qv500), and the vertical wind shear computed by the difference in horizontal wind vectors between 200 and 850 hPa (VWS). The SST, LHF, Qv925, and mCAPE were averaged within a radius of 200 km from the TC center. The Qv500 and VWS were averaged within a radius of 200–600 km to separate the influence of TC inner-core.

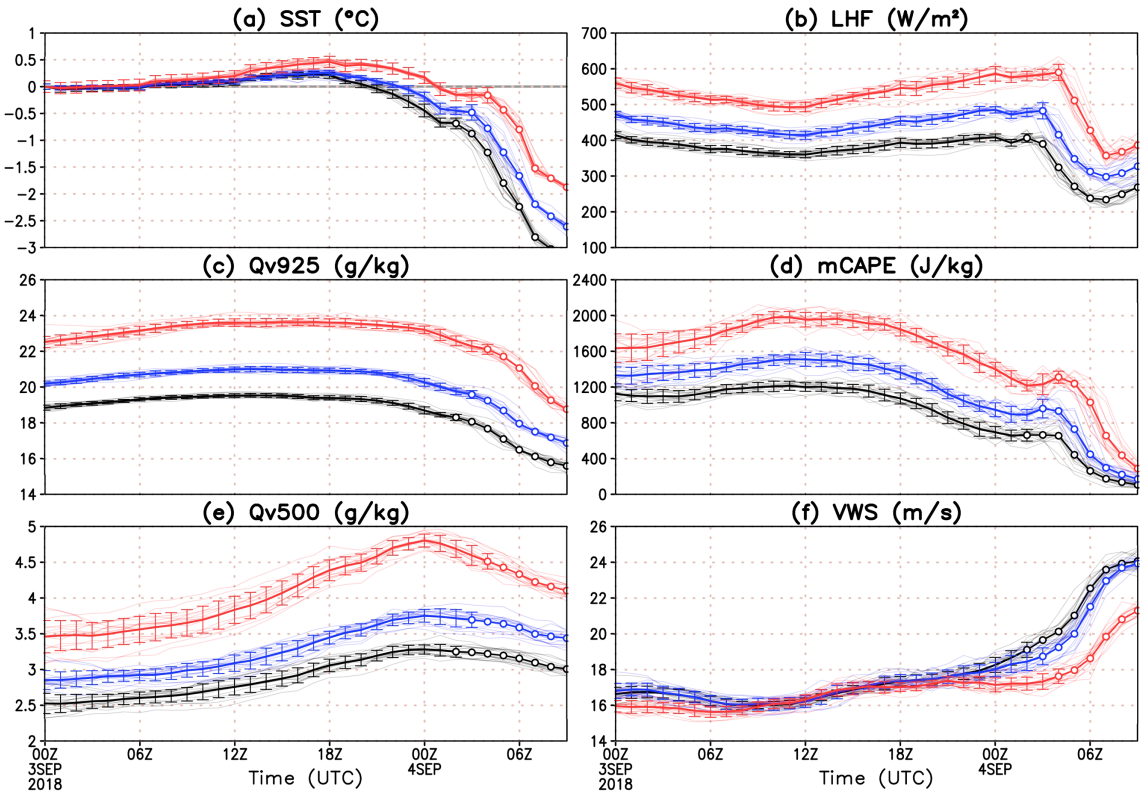

Fig. 6. (a) Time series of the SST averaged within a radius of 200 km from the TC center in the CTL (black line), PGW2 (blue line), and PGW4 (red line) runs. The SST is calculated as the difference from SST values at 0000 UTC on 3 September. Thin (thick) line denotes the value of each member (ensemble mean). Error bars denote the one standard deviation. Open marks indicate the time after landfall. (b–d) Same as in Fig. 6a but for the (b) LHF, (c) QV925, and (d) mCAPE. (e and f) Same as in Fig. 6a but for the (e) Qv500 and (f) VWS averaged within a radius of 200–600 km from the TC center.

The largely meridional increment of SST, as shown in Figs. 1b and 1c, created the warmer SST condition around Japan than the subtropical region along the TC track. The inner-core SST at 0000 UTC on 3 September was 28.48 ± 0.02, 29.70 ± 0.04, and 31.73 ± 0.04°C in the CTL, PGW2, and PGW4 runs. At the onset time of re-intensification (at 2000 UTC on 3 September), the CTL and PGW2 runs simulated almost the same SST values as in the subtropical region (Fig. 6a): 28.53 ± 0.05 and 29.81 ± 0.02°C, respectively. In the PGW4 run, the SST at the onset time (at 2200 UTC on 3 September), 32.11 ± 0.03°C, was higher by approximately 0.4°C than that at 0000 UTC on 3 September. Due to the large SST increase around Japan, re-intensified TCs in the PGW4 run gained abundant moisture from the underlying midlatitude ocean (Fig. 6b). This situation created a moist PBL and a large mCAPE in the inner core (Figs. 6c and 6d). For the middle troposphere, the environmental Qv500 around the TC increased significantly in the PGW4 run compared to those in the current and 2-K warming climates. These thermodynamic conditions in the lower and middle troposphere favored the development of deep eyewall convection. In addition, the warming-climate simulations, especially in the PGW4 run, showed a decrease of the VWS around TCs during the re-intensification phase. The low VWS in the PGW4 run may have originated from the deceleration of the upper-level jet due to the decrease in meridional temperature gradient through the geostrophic wind balance. Thus, we attributed the extreme changes in the intensity and axisymmetric structure of TCs derived from the PGW4 run to the combination of remarkable changes in thermodynamic environments (a remarkably warm ocean around Japan and lower-to-middle troposphere moistening) and the predominant VWS decrease in the midlatitudes under the 4-K warming future climate.

4. Summary

We investigated the effects of 2-K and 4-K warming future climates on the intensity and inner-core structure of Typhoon Jebi. Numerical simulations were carried out using the high-resolution WRF model: control runs with the current climate (CTL run) and PGW experiments with 2-K and 4-K warming climate conditions (PGW2 and PGW4 runs, respectively).

The PGW simulations showed the re-intensification over the ocean to the south of Japan. The re-intensification of Jebi was significant in the PGW4 run but was unclear in the PGW2 run. The maximum wind speed during the re-intensification phase increased by approximately 8% (20%) in the PGW2 (PGW4) run compared with that in the CTL run.

For the TC structures, the PGW4 run showed remarkable axisymmetric structures, such as the compact TC eye, deep eyewall convection and well-developed secondary circulation, around Japan. The secondary circulation accompanied by heavy precipitation within the eyewall contributed to the increase in cyclonic tangential flows through the large radial advection of absolute angular momentum. However, few differences were observed in the strength of secondary circulation between the PGW2 and CTL runs, leading to inner-core structures similar to those of the current climate experiments. The large differences in the TC intensity and structures between the two warming climate scenarios were caused by the enhanced ocean warming and troposphere moistening around Japan and a significant weakening of the VWS as a result of the climate changes in the 4-K global warming scenario.

The results of the present study suggest that the disaster risks associated with TCs increase at an accelerating rate due to TC development and maintenance of axisymmetric structures around Japan in response to the drastic climate changes in the 4-K warming scenario. In following next paper, we will discuss how the risks of Jebi-caused disasters increase in the 2-K and 4-K warmed climates. In addition, whether the nonlinear responses of Jebi to the warming scenario apply to other intense TCs remains unclear. Thus, additional numerical simulations are underway for several severe TCs that caused serious damage in Japan (e.g., Typhoons Faxai and Hagibis in 2019).

Acknowledgments

Comments and suggestions by Dr. Sachie Kanada and two anonymous reviewers were extremely useful. The NCEP FNL was obtained from online at https://rda.ucar.edu/datasets/ds083.2/. This study was conducted as collaborative research with AON. The study was also supported by the MEXT Advanced Studies of Climate Change Projection (SENTAN) Grant Number JPMXD0722678534 and JSPS Kakenhi 20H00289 and 23H00196.

Edited by: S. Kanada

Supplement

Supplement 1: Figs. S1–S4 and texts for Figs. S3 and S4.

References

DeMaria, M., and J. Kaplan, 1994: Sea surface temperature and the maximum intensity of Atlantic tropical cyclones. *J. Climate*, **7**, 1324–1334, doi:10.1175/1520-0442(1994)007%3C1324:SSTATM%3E2.0.CO;2.

Emanuel, K. A., 1988: The maximum intensity of hurricanes. *J. Atmos. Sci.*, **45**, 1143–1155, doi:10.1175/1520-0469(1988)045%3C1143:TMIOH%3E2.0.CO;2.

Dudhia, J., 1989: Numerical study of convection observed during the winter monsoon experiment using a mesoscale two-dimensional model. *J. Atmos. Sci.*, **46**, 3077–3107, doi:10.1175/1520-0469(1989)046%3C3077:NSOCOD%3E2.0.CO;2.

Fujita, M., R. Mizuta, M. Ishii, H. Endo, T. Sato, Y. Okada, S. Kawazoe, S. Sugimoto, K. Ishihara, and S. Watanabe, 2019: Precipitation changes in a climate with 2-K surface warming from large ensemble simulations using 60-km global and 20-km regional atmospheric models. *Geophys. Res. Lett.*, **46**, 435–442, doi:10.1029/2018GL079885.

Hong, S.-Y., 2010: A new stable boundary-layer mixing scheme and its impact on the simulated East Asia summer monsoon. *Quart. J. Roy. Meteor. Soc.*, **136**, 1481–1496, doi:10.1002/qj.665.

Hong, S.-Y., and J.-O. J. Lim, 2006: The WRF single-moment 6-class microphysics scheme (WSM6). *J. Korean Meteor. Soc.*, **42**, 129–151.

Hong, S.-Y., Y. Noh, and J. Dudhia, 2006: A new vertical diffusion package with an explicit treatment of entrainment processes. *Mon. Wea. Rev.*, **134**, 2318–2341, doi:10.1175/MWR3199.1.

IPCC. 2013. Climate Change 2013: The Physical Science Basis. *Contribution of Working Group I to the Fifth Assessment Report of the Intergovernmental Panel on Climate Change*. Cambridge University Press, Cambridge, UK and New York, NY, USA; 1535.

IPCC. 2014. Climate Change 2014: Impacts, Adaptation, and Vulnerability. Part A: Global and Sectoral Aspects. *Contribution of Working Group II to the Fifth Assessment Report of the Intergovernmental Panel on Climate Change*, Cambridge University Press, Cambridge, UK and New York, NY, USA; 1132.

Japan Meteorological Agency, 2018: Bulletin of Climate Monitoring 2017 (in Japanese). Accessed 10 January 2023, https://www.data.jma.go.jp/cpdinfo/monitor/.

Kanada, S., A. Wada, and M. Sugi, 2013: Future changes in structures of extremely intense tropical cyclones using a 2-km mesh nonhydrostatic model. *J. Climate*, **26**, 9986–10005, doi:10.1175/JCLI-D-12-00477.1.

Kanada, S., T. Takemi, M. Kato, S. Yamasaki, H. Fudeyasu, K. Tsuboki, O. Arakawa, and I. Takayabu, 2017: A multi-model intercomparison of an intense typhoon in future, warmer climates by four 5-km-mesh models. *J. Climate*, **24**, 6017–6036, doi:10.1175/JCLI-D-16-0715.1.

Kanada, S., K. Tsuboki, and I. Takayabu, 2020: Future changes of tropical cyclones in the midlatitudes in 4-km-mesh downscaling experiments from large-ensemble simulations. *SOLA*, **16**, 57–63, doi:10.2151/sola.2020-010.

Kossin, J., K. Emanuel, and G. Vecchi, 2014: The poleward migration of the location of tropical cyclone maximum intensity. *Nature*, **509**, 349–352, doi:10.1038/nature13278.

Kossin, J., K. Emanuel, and G. Vecchi, 2016: Past and projected changes in Western North Pacific tropical cyclone exposure. *J. Climate*, **29**, 5725–5739, doi:10.1175/JCLI-D-16-0076.1.

Miyamoto, Y., and T. Takemi, 2013: A transition mechanism for the spontaneous axisymmetric intensification of tropical cyclones. *J. Atmos. Sci.*, **70**, 112–129, doi:10.1175/JAS-D-11-0285.1.

Mizuta, R., H. Yoshimura, H. Murakami, M. Matsueda, H. Endo, T. Ose, K. Kamiguchi, M. Hosaka, M. Sugi, S. Yukimoto, S. Kusunoki, and A. Kitoh, 2012: Climate simulations using MRI-AGCM3.2 with 20-km grid. *J. Meteor. Soc. Japan*, **90A**, 233–258, doi:10.2151/jmsj.2012-A12.

Mizuta, R., and co-authors, 2017: Over 5000 years of ensemble future climate simulations by 60 km global and 20 km regional atmospheric models. *Bull. Amer. Meteor. Soc.*, 1383–1398, doi:10.1175/BAMS-D-16-0099.1.

Mlawer, E. J., S. J. Taubman, P. D. Brown, M. J. Iacono, and S. A. Clough, 1997: Radiative transfer for inhomogeneous atmospheres: RRTM a validated correlated-k model for the longwave. *J. Geophys. Res.*, **102**, 16663–16682, doi:10.1029/97JD00237.

Mori, N., T. Yasuda, T. Arikawa, T. Kataoka, S. Nakajo, K. Suzuki, Y. Yamanaka, and A. Webb, 2019: 2018 Typhoon Jebi post-event survey of coastal damage in the Kansai region, Japan. *Coastal Eng. J.*, **61**, 278–294, doi:10.1080/21664250.2019.1619253.

Murakami, H., Y. Wang, H. Yoshimura, R. Mizuta, M. Sugi, E. Shindo, Y. Adachi, S. Yukimoto, M. Hosaka, S. Kusunoki, T. Ose, and A. itoh, 2012: Future changes in tropical cyclone activity projected by the new high-resolution MRI-AGCM. *J. Climate*, **25**, 3237–3260, doi:10.1175/JCLI-D-11-00415.1.

Murakami, H., and M. Sugi, 2010: Effect of model resolution on tropical cyclone climate projections. *SOLA*, **6**, 73–76, doi:10.2151/sola.2010-019.

Nayak, S., and T. Takemi, 2019: Dynamical downscaling of Typhoon Lionrock (2016) for assessing the resulting hazards under global warming. *J. Meteor. Soc. Japan*, **97**, 69–88, doi:10.2151/jmsj.2019-003.

Oouchi, K., J. Yoshimura, H. Yoshimura, R. Mizuta, S. Kusunoki, and A. Noda, 2006: Tropical cyclone climatology in a global-warming climate as simulated in a 20-km-mesh global atmospheric model: Frequency and intensity analysis. *J. Meteor. Soc. Japan*, **84**, 259–276, doi:10.2151/jmsj.84.259.

Skamarock, W. C., J. B. Klemp, J. Dudhia, D. O. Gill, D. M. Barker, M. G. Duda, X. Y. Huang, W. Wang, and J. G. Powers, 2008: *A Description of the Advanced Research WRF Version 3*. NCAR Tech. Note, National Center for Atmospheric Research, USA, 13 pp, doi:10.5065/D68S4MVH.

Takemi, T., 2012: Projected regional-scale changes in atmospheric stability condition for the development of summertime convective precipitation in the Tokyo metropolitan area under global warming. *Hydrol. Res. Lett.*, **6**, 17–22, doi:10.3178/hrl.6.17.

Takemi, T., 2019: Impacts of global warming on extreme rainfall of a slow-moving typhoon: A case study for Typhoon Talas (2011). *SOLA*, **15**, 125–131, doi:10.2151/sola.2019-023.

Takemi, T., Y. Okada, R. Ito, H. Ishikawa, and E. Nakakita, 2016: Assessing the impacts of global warming on meteorological hazards and risks in Japan: Philosophy and achievements of the SOUSEI program. *Hydrol. Res. Lett.*, **10**, 119–125, doi:10.3178/hrl.10.119.

Takemi, T., T. Yoshida, S. Yamasaki, and K. Hase, 2019: Quantitative estimation of strong winds in an urban district during Typhoon Jebi (2018) by merging mesoscale meteorological and large-eddy simulations. *SOLA*, **15**, 22–27, doi:10.2151/sola.2019-005.

Tsuboki, K., M. K. Yoshioka, T. Shinoda, M. Kato, S. Kanada, and A. Kitoh, 2015: Future increase of supertyphoon intensity associated with climate change. *Geophys. Res. Lett.*, **42**, 646–652, doi:10.1002/2014GL061793.

Wang, C.-C., B.-X. Lin, C.-T. Chen, and S.-H. Lo, 2015: Quantifying the effects of long-term climate change on tropical cyclone rainfall using a cloud-resolving model: Examples of two landfall typhoons in Taiwan. *J. Climate*, **28**, 66–85, doi:10.1175/JCLI-D-14-00044.1.

Yoshida, K., M. Sugi, R. Mizuta, H. Murakami, and M. Ishii, 2017: Future changes in tropical cyclone activity in high-resolution large-ensemble simulations. *Geophys. Res. Lett.*, **44**, 9910–9917, doi:10.1002/2017GL075058.